Radiology

Endoleak and In-Stent Thrombus Detection with CT Angiography in a Thoracic Aortic Aneurysm Phantom at Different Tube Energies Using Filtered Back Projection and Iterative Algorithms[1]

Zsuzsanna Deák, MD
Jochen M. Grimm, MD
Fabian Mueck, MD
Lucas L. Geyer, MD
Marcus Treitl, MD
Maximilian F. Reiser, MD
Stefan Wirth, PhD, MD

Purpose: To determine the lower limit of dose reduction with hybrid and fully iterative reconstruction algorithms in detection of endoleaks and in-stent thrombus of thoracic aorta with computed tomographic (CT) angiography by applying protocols with different tube energies and automated tube current modulation.

Materials and Methods: The calcification insert of an anthropomorphic cardiac phantom was replaced with an aortic aneurysm model containing a stent, simulated endoleaks, and an intraluminal thrombus. CT was performed at tube energies of 120, 100, and 80 kVp with incrementally increasing noise indexes (NIs) of 16, 25, 34, 43, 52, 61, and 70 and a 2.5-mm section thickness. NI directly controls radiation exposure; a higher NI allows for greater image noise and decreases radiation. Images were reconstructed with filtered back projection (FBP) and hybrid and fully iterative algorithms. Five radiologists independently analyzed lesion conspicuity to assess sensitivity and specificity. Mean attenuation (in Hounsfield units) and standard deviation were measured in the aorta to calculate signal-to-noise ratio (SNR). Attenuation and SNR of different protocols and algorithms were analyzed with analysis of variance or Welch test depending on data distribution.

Results: Both sensitivity and specificity were 100% for simulated lesions on images with 2.5-mm section thickness and an NI of 25 (3.45 mGy), 34 (1.83 mGy), or 43 (1.16 mGy) at 120 kVp; an NI of 34 (1.98 mGy), 43 (1.23 mGy), or 61 (0.61 mGy) at 100 kVp; and an NI of 43 (1.46 mGy) or 70 (0.54 mGy) at 80 kVp. SNR values showed similar results. With the fully iterative algorithm, mean attenuation of the aorta decreased significantly in reduced-dose protocols in comparison with control protocols at 100 kVp (311 HU at 16 NI vs 290 HU at 70 NI, $P \leq .0011$) and 80 kVp (400 HU at 16 NI vs 369 HU at 70 NI, $P \leq .0007$).

Conclusion: Endoleaks and in-stent thrombus of thoracic aorta were detectable to 1.46 mGy (80 kVp) with FBP, 1.23 mGy (100 kVp) with the hybrid algorithm, and 0.54 mGy (80 kVp) with the fully iterative algorithm.

Online supplemental material is available for this article.

[1] From the Department for Clinical Radiology, Ludwig-Maximilians-University, Campus Innenstadt, Nussbaumstrasse 20, 80336 Munich, Germany (Z.D., F.M., L.L.G., M.T., M.F.R., S.W.); and Departments of Medical Radiology and Legal Medicine, University Hospital of Lausanne, Lausanne, Switzerland (J.M.G.). Received March 28, 2013; revision requested May 28; revision received August 11; accepted August 29; final version accepted November 6. **Address correspondence to** Z.D. (e-mail: *zsuzsanna.deak@med.uni-muenchen.de*).

Endovascular aortic aneurysm repair (EVAR) is an accepted alternative to open surgical repair in the treatment of thoracic aortic aneurysms (1–3). There are, however, important complications—such as endoleak formation, aneurysm expansion, or stent failure—that require life-long imaging surveillance. Contrast material–enhanced computed tomographic (CT) angiography is a rapid and easily available imaging method that depicts aortic aneurysms not only in the preoperative planning phase but also after EVAR. CT angiography can be used to detect endoleaks with a high degree of sensitivity. Furthermore, the volumetric data sets of isotropic voxels offer thin-section multiplanar reformatted images and enable accurate and reproducible volume and diameter measurement of the aneurysm sac (4–7). However, because patients require multiple follow-up studies after EVAR, the high cumulative dose of ionizing radiation is of concern (8). Software developments, including advanced image reconstruction algorithms, permit a substantial decrease in CT radiation dose when compared with examinations performed a decade ago (8). Partially iterative hybrid algorithms have been used since 2009 and have been reported to significantly decrease patient radiation dose in comparison with filtered back projection (FBP), which had been known as a well-established standard reconstruction algorithm (9–13). Model-based iterative reconstruction (MBIR), a fully iterative algorithm that models noise statistics and the parameters of the machine itself, shows considerable dose reduction potential in CT imaging of the chest, abdomen, and coronary arteries (9,14–19). The use of reduced tube energy for CT angiography is an attractive method with which to improve vessel attenuation and reduce patient exposure to radiation; however, the associated increase in image noise represents a potential problem, impairing the detection of small objects like endoleaks (20,21). Iterative algorithms could potentially compensate for the increased image noise, allowing for endoleak and in-stent thrombus detection without loss of diagnostic confidence.

The purpose of this phantom study was to assess the lower limit of dose reduction with hybrid and fully iterative reconstruction algorithms for detectability of endoleak and in-stent thrombus of the thoracic aorta by applying CT angiography protocols of different tube energies and automated tube current modulation.

Advances in Knowledge

- Endoleaks and in-stent thrombus of the thoracic aorta were detectable in our phantom with filtered back projection (FBP) at a higher noise level (signal-to-noise ratio [SNR], 5.5) than recommended by the manufacturer (SNR, 9.5) at 120 kVp.
- At 80 kVp in our phantom, medium endoleaks (>100 mm^2) were identified even at a highly increased image noise level at 95% less radiation exposure (CT dose index, 8.49 mGy at 120 kVp vs 0.54 mGy at 80 kVp) with FBP and the hybrid algorithm; however, smaller endoleaks (≤100 mm^2) were not seen.
- In our phantom, radiation dose was reduced by 66%, 69%, and 63% at 120, 100, and 80 kVp, respectively, with the fully iterative algorithm in comparison with FBP, without loss of accuracy in endoleak and thrombus detection.
- In the images reconstructed with the fully iterative algorithm, mean attenuation of the aorta significantly decreased in the reduced-dose protocols at 100 kVp and 80 kVp by up to 21 HU and 31 HU, respectively ($P \leq .001$).

Implications for Patient Care

- In comparison to FBP, the fully iterative reconstruction algorithm appears to be a reliable method with which to detect endoleaks and in-stent thrombus at substantially reduced radiation exposure, especially with the aid of low-kilovoltage CT angiographic protocols.
- Prolonged reconstruction time of the fully iterative algorithm limits its use to nonemergency cases in everyday radiology practice.

Materials and Methods

Phantom Design

The original cylindrical calcification insert (diameter, 100 mm) of an anthropomorphic cardiac phantom (QRM-Cardio-Phantom; QRM, Moehrendorf, Germany) 200 mm in anterior-posterior diameter and 300 mm in lateral diameter was replaced with a cylindrical plastic case (diameter, 85 mm) containing a self-expanding aortic stent graft (Vanguard; Boston Scientific, Natick, Mass). The phantom had an artificial spine insert and a shell made of soft-tissue-equivalent material mimicking the human thorax with respect to attenuation characteristics.

Published online before print
10.1148/radiol.13130740 **Content codes:** VA CT

Radiology 2014; 271:574–584

Abbreviations:
ASIR = adaptive statistical iterative reconstruction
EVAR = endovascular aortic aneurysms repair
FBP = filtered back projection
MBIR = model-based iterative reconstruction
NI = noise index
SNR = signal-to-noise ratio

Author contributions:
Guarantors of integrity of entire study, Z.D., F.M., M.T., S.W.; study concepts/study design or data acquisition or data analysis/interpretation, all authors; manuscript drafting or manuscript revision for important intellectual content, all authors; approval of final version of submitted manuscript, all authors; literature research, Z.D., L.L.G., M.T., M.F.R.; experimental studies, Z.D., J.M.G., L.L.G., M.T., S.W.; statistical analysis, Z.D., F.M., M.T.; and manuscript editing, Z.D., J.M.G., F.M., M.T., M.F.R., S.W.

Conflicts of interest are listed at the end of this article.

Figure 1

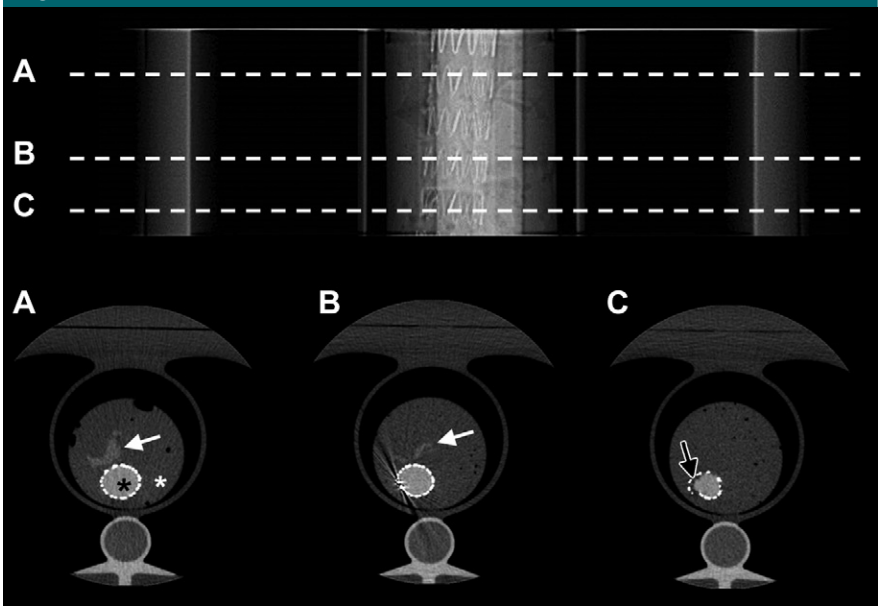

Figure 1: Phantom design. Top: Anteroposterior scout view of the phantom. *A*, *B*, and *C* indicate the level at which axial images were obtained and correspond to *A*, *B*, and *C* in the companion image. Bottom: Sample axial images. White arrows in, *A*, and, *B*, indicate endoleaks. *C*, Black arrow indicates the in-stent thrombus. The lumen of the aorta (black ∗) and the aneurysm (white ∗) can be seen.

The flacon modeling the aortic aneurysm was placed directly next to the artificial spine and filled with a gel composed of ferrous (II) glycine sulfate complex, sucrose, and ultrasonograhy (US) gel (Sonosid; Asid Bonz, Herrenberg, Germany) to mimic thrombus material.

A thin plastic sheath containing a dilution of contrast material (Solutrast 300; Bracco Imaging, Konstanz, Germany) and physiologic saline solution inserted into the aortic stent represented the aortic lumen after EVAR. A second thin and amorphous sheath of a dilution of contrast material and physiologic saline solution placed next to the stent graft simulated the endoleaks. The mean (± standard deviation) attenuation of the endoleak and graft lumen were adjusted to the attenuation measured in 15 patients with follow-up CT angiography after EVAR; these were 144 HU ± 2.7 and 246.5 HU ± 2.5, respectively. The three highest attenuation values measured in the thrombus of the aneurysm were selected to determine thrombus attenuation; the mean attenuation was 55.4 HU ± 1.4.

In general, the sheath lay tight against the stent graft; however, there remained a thin space between the graft and sheath in some places. The gel mimicking the thrombus material of the aneurysm also was located in this space, and it formed a parietal in-stent thrombus inside the stent graft. The width of this pseudothrombus was 2–3 mm (Fig 1).

Before the phantom was built, the filling materials mimicking the thrombus, aorta, and endoleaks were titrated for attenuation level.

CT System Parameters

Imaging was performed with a 64-row multidetector CT scanner (HD 750 Discovery; GE Healthcare, Waukesha, Wis). The tube current in modern CT scanners is controlled by an automated tube current modulation program to reduce the overall patient dose and maintain a predefined quantum noise level in the image data. The system also allows the operator to define the range within which the tube current can be modulated by selecting the minimum and maximum amperage. The upper limit can prevent an excessive radiation dose at the cost of image quality in obese patients. This means that the tube current does not exceed the threshold, even if the quantum noise level in the image data is higher than desired (22).

The multidetector CT scanner controls image noise level via the operator-selected noise index (NI), which refers to the operator-selected primary reconstruction section thickness (0.625, 1.25, 2.5, 3.75, and 5 mm) and FBP algorithm. The NI optimizes the tube current to adapt radiation exposure to the patient's geometry along the z-axis and in the x-y plane. This issue is discussed in Appendix E1 (online) and in articles by Kanal et al (23) and Söderberg and Gunnarsson (24).

In general, image noise is inversely proportional to the square root of the section thickness. For example, an NI of 70 with a section thickness of 0.625 mm corresponds to an NI of 35 with a section thickness of 2.5 mm. Consequently, operator-selected section thickness has to be increased to realize the NI-guided tube current modulation desired at higher image noise levels (14,23,24).

In this study, a primary reconstruction section thickness of 2.5 mm was chosen, and images with a section thickness of 0.625 mm were retrospectively reconstructed with *(a)* FBP, *(b)* the hybrid adaptive statistical iterative reconstruction (ASIR) algorithm with a 50% blending factor and section mode (ASiR; GE Healthcare), and *(c)* the MBIR technique, which is a fully iterative algorithm (Veo; GE Healthcare). All the images were reconstructed with a soft-tissue kernel and reformatted with intervals of 1.25 mm and 2.5 mm for evaluation. Reconstruction time was recorded for each algorithm.

The phantom was scanned with tube energies of 80, 100, and 120 kVp. The lower and upper thresholds of the tube current were 4 and 750

mAs, respectively. Additional scanning parameters were 2.5-mm primary reconstruction section thickness, 64 × 0.625-mm detector collimation, 0.4-second rotation time, and 0.984:1 pitch. The NI of 16 at a section thickness of 2.5 mm is equal to an NI of 32 at a section thickness of 0.625 mm, which is consistent with the manufacturer recommendations for CT angiography for images acquired at 120 kVp and reconstructed with FBP. At each tube energy, data sets were acquired with seven protocols by using incrementally increasing NIs of 16, 25, 34, 43, 52, 61, and 70. The manufacturer's specification recommends the application of an NI of 16 in combination with a primary reconstruction section thickness of 2.5 mm for CT angiography of the thorax. In our study, the protocol in which an NI of 16 was used served as a common control regarding endoleak and thrombus identification, as well as noise and CT attenuation measurements. Axial images with a 1.25-mm interval and those with a 2.5-mm section thickness were evaluated.

The dose values were recorded as CT dose index, and the values of size-specific dose estimate referring to the effective diameter of the phantom (24.49 cm) were calculated according to the American Association of Physicists in Medicine report number 204 (25). The corresponding conversion factor was 1.53.

Assessment of Detectibility of Simulated Endoleaks and In-Stent Thrombus

The simulated endoleaks showed variable configurations due to the random form of the liquid-filled sheath placed in the gel. The larger diameter of the endoleaks varied from 5 to 26 mm, and the smaller diameter varied from 3 to 20 mm, as measured on the control FBP images. Endoleaks were divided in two groups according to axial dimension: small endoleaks were those smaller than 50 mm^2, and medium endoleaks were those larger than 100 mm^2. Altogether, 21 images with small endoleaks of different configurations and 15 images of medium endoleaks were identified. The thickness of the in-stent thrombus varied from 2 to 3 mm.

At each tube energy (n = 3) for each reduced-dose scan (n = 6) and each reconstruction algorithm (n = 3), four images were selected—one with a small endoleak, one with a medium endoleak, one with a thrombus, and one without an endoleak or a thrombus—that correspond to 72 images for a single reconstruction algorithm (ie, 3 × 6 × 4 = 72). Endoleaks of variable configuration but similar size were chosen to decrease the number of repeated images. Images without lesions served as negative control images. The images were independently presented one at a time to five radiologists (F.M., M.T., S.W., and two other radiologists; 1–10 years of experience) who were blinded to reconstruction and scanning parameters.

The presentation of images started with the protocols with NIs of 52, 61, and 70 and finished with the protocols with NIs of 25, 34, and 43. The images from two dose ranges from 0.41 mGy (NI = 70) to 1.02 mGy (NI = 52) and from 1.16 mGy (NI = 43) to 4.4 mGy (NI = 25) were presented in random order. Radiologists had to answer two questions with a response of *yes*, *no* or *maybe*. The questions were as follows: Is there any in-stent thrombus in the image? Are there any endoleaks in the image? In case of a positive answer, the observers had to communicate the location of the lesions. The study conductor (Z.D.), who was aware of the exact location of the lesions, recorded the answers and classified them as true-positive, false-positive, true-negative, or false-negative. Unsure answers (a response of *maybe*) were automatically interpreted as false for the calculation of both sensitivity and specificity. Sensitivity was 5 of 5 if all five radiologists accurately identified the lesion. Specificity was 5 of 5 if all five radiologists properly excluded the lesion.

Readers evaluated single images to decrease the effect of reading adjacent sections, which usually ease the interpretation of image findings in a clinical situation (26). Window center and width were 200 and 600 HU, respectively.

Measurements of Signal-To-Noise Ratio of the Aorta

Circular 10-mm-diameter regions of interest were drawn in the aorta on the 0.625-mm images to avoid partial volume averaging. Measurements were performed at an advanced workstation (Advantage Workstation; GE Healthcare). Mean attenuation value (in Hounsfield units) and standard deviation were recorded, and signal-to-noise ratio (SNR) was calculated. The size and position of regions of interest were kept constant in each study; measurements were repeated 10 times for each exposure and reconstruction combination by using different section positions. Image noise was defined as the standard deviation of the CT numbers.

Statistical Analysis

The data of the attenuation values and the SNR measurements were compared by using one-way analysis of variance. Attenuation of the aorta measured in low-dose protocols was compared with the corresponding attenuation measured in the control protocol with the same reconstruction algorithm and tube energy. SNR values measured on ASIR and MBIR images obtained with the low-dose protocols were compared with SNR values on FBP images of the control protocol within the same tube energy level. First, the data were tested with the Levene test for homogeneity of distribution. In the case of inhomogeneous data distribution, analysis of variance was replaced with the Welch test.

The Tukey honestly significant difference test and the Games-Howell test were used as post hoc tests in the case of homogeneous or inhomogeneous data distribution, respectively (27). The level of significance was set at $P < .05$. With the aid of Bonferroni correction, the confidence interval was adjusted for the Games-Howell

Table 1

Dose Values

Tube Energy and Noise Index	CT Dose Index (mGy)	Size-specific Dose Estimate (mGy)	Tube Current Time Product (mAs)	
			Effective Value	Range
120 kVp				
16*	8.49	12.99	110	100–112
25	3.45	5.28	44	40–45
34	1.83	2.80	24	22–25
43	1.16	1.77	15	13–15
52	0.78	1.19	10	9–10
61	0.56	0.86	8	7–8
70	0.41	0.63	6	5–6
100 kVp				
16*	9.11	13.94	186	166–189
25	3.68	5.63	75	69–77
34	1.98	3.03	40	38–42
43	1.23	1.88	24	23–26
52	0.84	1.29	17	16–18
61	0.61	0.93	12	11–13
70	0.46	0.70	8	8–9
80 kVp				
16*	10.53	16.11	405	377–410
25	4.40	6.73	169	149–174
34	2.32	3.55	88	84–90
43	1.46	2.23	54	50–56
52	1.02	1.56	40	34–42
61	0.74	1.13	28	26–29
70	0.54	0.83	20	18–21

* Control protocol.

and Welch test, and the significance level was set at 0.0083 (0.05/6 = 0.0083).

For all three reconstruction algorithms, the threshold of the SNR values was determined by using binary logistic regression analysis.

With respect to the five readers' answers, the outcome was coded as 1 in case of true-positive (5/5) and true-negative (5/5) answers and as 0 if the answers were inconsistent. Separately for both thrombus and small endoleak detection, threshold values maximizing sensitivity and specificity were identified with receiver operating characteristic analysis and the Youden index.

Statistical software (SPSS, version 19.0.0; IBM, Armonk, NY) was used for all calculations.

Results

Dose values of the protocols and the corresponding tube current parameters are shown in Table 1.

The mean image reconstruction time was 15.5 seconds (range, 10.5–24.6 seconds) for FBP, 16.8 seconds (range, 12.6–25.4 seconds) for ASIR, and 14.7 minutes (range, 10.8–28.5 minutes) for MBIR.

Detectability of Simulated Endoleak and In-Stent Thrombus

The data on lesion conspicuity are detailed in Tables 2 and 3. Increased section thickness improved lesion conspicuity, especially for simulated endoleaks. With the aid of sensitivity and specificity values for both endoleak and in-stent thrombus detectability, sufficient noise and corresponding dose levels were identified for each algorithm at each tube energy. Figure 2 shows a summary of the sufficient dose levels for the 2.5-mm images.

Endoleak conspicuity.—At 80 kVp, medium endoleaks were detectable at minimal radiation dose (0.54 mGy) with all three algorithms on the 2.5-mm images (Fig 3). The use of higher tube energies required increased radiation dose to depict medium endoleaks. However, at 80 kVp, the small endoleaks were poorly visualized on FBP and ASIR images. On the 2.5-mm images, small endoleaks were reliably identified by all five readers on FBP, ASIR, and MBIR images by using NIs of 25, 34, and 52, respectively, at 120 kVp; NIs of 34, 43, and 70, respectively, at 100 kVp; and NIs of 43, 43, and 70, respectively, at 80 kVp.

Detection of in-stent thrombus.—With FBP or ASIR, the simulated in-stent thrombus was detectable in most cases at a lower dose level than that required for endoleaks. At 120, 100, and 80 kVp, thrombus detection was sufficient with noise indexes of 34, 43, and 52, respectively, for FBP and 34, 52, and 61, respectively, for ASIR on 2.5-mm images. However, on MBIR images, thrombus detection required NIs of 43, 61, and 70 at 120, 100, and 80 kVp, respectively, that corresponded to higher dose levels at 120 and 100 kVp than for endoleak detection. For example, with NIs of 52 at 120 kV and 70 at 100 kV, endoleaks were identified with high sensitivity (5/5) and specificity (5/5); however, some observers interpreted the hypodense areas of the blotchy image appearance as thrombus, resulting in false-positive answers and low specificity (3/5) even if real in-stent thrombus was detected with high sensitivity (5/5) (Fig 4).

Signal and Noise Measurements

The signal and noise measurements are summarized in Table 4.

Attenuation.—The mean CT attenuation measured in the aorta showed no significant difference for the reduced-dose protocols on FBP and ASIR images obtained with different tube energies. The mean attenuation measured in the aorta significantly decreased at

Table 2

Endoleak Sensitivity and Specificity for Each Protocol

Tube Energy and NI	Sensitivity												Specificity					
	Medium Endoleaks						Small Endoleaks						Small Endoleaks					
	1.5 mm			2.5 mm			1.5 mm			2.5 mm			1.5 mm			2.5 mm		
	FBP	ASIR	MBIR	FBP	ASIR	MBIR	FBP	ASIR	MBIR	FBP	ASIR	MBIR	FBP	ASIR	MBIR	FBP	ASIR	MBIR
120 kVp																		
16	NA	NA	NA	NA	NA	NA	NA	NA	NA	NA	NA	NA	NA	NA	NA	NA	NA	NA
25	5/5*	5/5*	5/5*	5/5*	5/5*	5/5*	5/5*	5/5*	5/5*	5/5*	5/5*	5/5*	5/5	5/5	5/5	5/5	5/5	5/5
34	5/5*	5/5*	5/5*	5/5*	5/5*	5/5*	1/5	2/5	5/5*	2/5	5/5*	5/5*	3/5	5/5	5/5	4/5	5/5	5/5
43	5/5*	5/5*	5/5*	5/5*	5/5*	5/5*	0/5	0/5	5/5*	0/5	1/5	5/5*	3/5	4/5	5/5	3/5	4/5	5/5
52	1/5	1/5	5/5*	2/5	3/5	5/5*	0/5	0/5	4/5	0/5	0/5	5/5*	3/5	3/5	5/5	3/5	3/5	5/5
61	0/5	1/5	5/5*	1/5	1/5	5/5*	0/5	0/5	0/5	0/5	0/5	2/5	3/5	3/5	4/5	3/5	3/5	4/5
70	0/5	0/5	2/5	0/5	0/5	2/5	0/5	0/5	0/5	0/5	0/5	0/5	3/5	3/5	4/5	3/5	3/5	4/5
100 kVp																		
16	NA	NA	NA	NA	NA	NA	NA	NA	NA	NA	NA	NA	NA	NA	NA	NA	NA	NA
25	5/5*	5/5*	5/5*	5/5*	5/5*	5/5*	5/5*	5/5*	5/5*	5/5*	5/5*	5/5*	5/5	5/5	5/5	5/5	5/5	5/5
34	5/5*	5/5*	5/5*	5/5*	5/5*	5/5*	5/5*	5/5*	5/5*	5/5*	5/5*	5/5*	5/5	5/5	5/5	5/5	5/5	5/5
43	5/5*	5/5*	5/5*	5/5*	5/5*	5/5*	0/5	4/5	5/5*	3/5	5/5*	5/5*	5/5	5/5	5/5	5/5	5/5	5/5
52	4/5	4/5	5/5*	5/5*	5/5*	5/5*	0/5	0/5	5/5*	1/5	2/5	5/5*	3/5	3/5	5/5	4/5	4/5	5/5
61	0/5	2/5	5/5*	3/5	4/5	5/5*	0/5	0/5	5/5*	0/5	0/5	5/5*	3/5	3/5	5/5	3/5	3/5	5/5
70	0/5	1/5	5/5*	1/5	1/5	5/5*	0/5	0/5	4/5	0/5	0/5	5/5*	3/5	3/5	4/5	3/5	3/5	5/5
80 kVp																		
16	NA	NA	NA	NA	NA	NA	NA	NA	NA	NA	NA	NA	NA	NA	NA	NA	NA	NA
25	5/5*	5/5*	5/5*	5/5*	5/5*	5/5*	5/5*	5/5*	5/5*	5/5*	5/5*	5/5*	5/5	5/5	5/5	5/5	5/5	5/5
34	5/5*	5/5*	5/5*	5/5*	5/5*	5/5*	5/5*	5/5*	5/5*	5/5*	5/5*	5/5*	5/5	5/5	5/5	5/5	5/5	5/5
43	5/5*	5/5*	5/5*	5/5*	5/5*	5/5*	5/5*	5/5*	5/5*	5/5*	5/5*	5/5*	5/5	5/5	5/5	5/5	5/5	5/5
52	5/5*	5/5*	5/5*	5/5*	5/5*	5/5*	1/5	3/5	5/5*	2/5	4/5	5/5*	5/5	5/5	5/5	5/5	5/5	5/5
61	5/5*	5/5*	5/5*	5/5*	5/5*	5/5*	0/5	0/5	5/5*	0/5	1/5	5/5*	3/5	3/5	5/5	4/5	4/5	5/5
70	5/5*	5/5*	5/5*	5/5*	5/5*	5/5*	0/5	0/5	5/5*	0/5	0/5	5/5*	3/5	3/5	4/5	3/5	3/5	5/5

Note.—Sensitivity is given as the number of true-positive answers per all answers for the five readers for both small and medium endoleaks.

* Images of high sensitivity or specificity for thrombus detection.

Table 3

Thrombus Sensitivity and Specificity for Each Protocol

Tube Energy and NI	Sensitivity						Specificity					
	1.25 mm			2.5 mm			1.25 mm			2.5 mm		
	FBP	ASIR	MBIR	FBP	ASIR	MBIR	FBP	ASIR	MBIR	FBP	ASIR	MBIR
120 kVp												
16	NA	NA	NA	NA	NA	NA	NA	NA	NA	NA	NA	NA
25	5/5*	5/5*	5/5*	5/5*	5/5*	5/5*	5/5	5/5	5/5	5/5	5/5	5/5
34	5/5*	5/5*	5/5*	5/5*	5/5*	5/5*	5/5	5/5	5/5	5/5	5/5	5/5
43	3/5	4/5*	5/5*	4/5	5/5*	5/5*	2/5	2/5	5/5	2/5	5/5	5/5
52	2/5	1/5	5/5*	3/5	3/5	5/5*	2/5	2/5	3/5	2/5	3/5	3/5
61	2/5	1/5	4/5	2/5	2/5	4/5	2/5	2/5	3/5	2/5	2/5	3/5
70	2/5	1/5	3/5	2/5	2/5	3/5	1/5	1/5	2/5	1/5	1/5	3/5
100 kVp												
16	NA	NA	NA	NA	NA	NA	NA	NA	NA	NA	NA	NA
25	5/5*	5/5*	5/5*	5/5*	5/5*	5/5*	5/5	5/5	5/5	5/5	5/5	5/5
34	5/5*	5/5*	5/5*	5/5*	5/5*	5/5*	5/5	5/5	5/5	5/5	5/5	5/5
43	5/5*	5/5*	5/5*	5/5*	5/5*	5/5*	5/5	5/5	5/5	5/5	5/5	5/5
52	3/5	4/5	5/5*	4/5	5/5*	5/5*	4/5	5/5	5/5	4/5	5/5	5/5
61	3/5	3/5	5/5*	3/5	3/5	5/5*	3/5	3/5	5/5	3/5	3/5	5/5
70	1/5	1/5	5/5*	1/5	2/5	5/5*	3/5	3/5	3/5	3/5	3/5	3/5
80 kVp												
16	NA	NA	NA	NA	NA	NA	NA	NA	NA	NA	NA	NA
25	5/5*	5/5*	5/5*	5/5*	5/5*	5/5*	5/5	5/5	5/5	5/5	5/5	5/5
34	5/5*	5/5*	5/5*	5/5*	5/5*	5/5*	5/5	5/5	5/5	5/5	5/5	5/5
43	5/5*	5/5*	5/5*	5/5*	5/5*	5/5*	5/5	5/5	5/5	5/5	5/5	5/5
52	5/5*	5/5*	5/5*	5/5*	5/5*	5/5*	5/5	5/5	5/5	5/5	5/5	5/5
61	3/5	5/5*	5/5*	3/5	5/5*	5/5*	5/5	5/5	5/5	5/5	5/5	5/5
70	1/5	2/5	5/5*	2/5	2/5	5/5*	3/5	3/5	5/5	4/5	4/5	5/5

Note.—An NI of 16 was used as the control. NA = not applicable.

* Images of high sensitivity or specificity for thrombus detection.

Figure 2

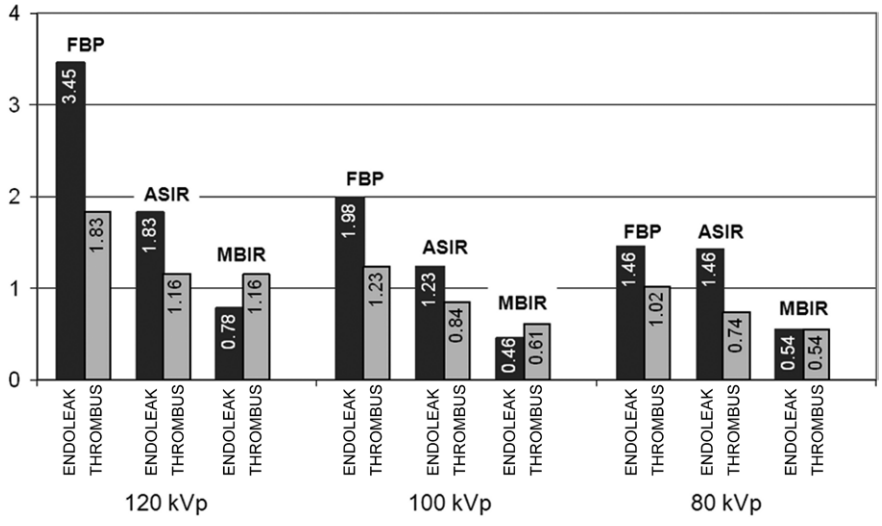

Figure 2: Graph shows summary of suggested dose levels to optimize performance. The y-axis represents radiation dose (CT dose index, in milligrays). The columns show the necessary radiation dose to detect simulated endoleak and in-stent thrombus with high sensitivity (5/5) and specificity (5/5) applying different tube energies and algorithms.

lower dose levels both at 100 kVp and at 80 kVp on MBIR images. The corresponding *P* values are listed in Table 4.

SNR.—Image noise increased gradually in the reduced-dose protocols, leading to gradually decreasing SNR of the aorta at each tube energy for all algorithms. However, SNR for the MBIR images in the reduced-dose protocols did not decrease below SNR for the control FBP images.

Accurate detection of endoleaks and in-stent thrombus was possible in only those images obtained with reduced-dose protocols in which SNR values of the aorta reached a certain threshold. For FBP and ASIR images, the threshold SNR values were 5.5 (sensitivity, 0.989; specificity, 0.992; area under the receiver operating characteristic curve [AUC], 0.999; $P < .0001$) and 6.6 (sensitivity, 0.973; specificity, 0.950; AUC, 0.994; $P < .0001$), respectively, for endoleak detection and 5.1 (sensitivity, 0.955; specificity, 0.920; AUC, 0.989; $P < .0001$) and 4.7 (sensitivity, 0947; specificity, 0.950; AUC, 0.992; $P < .0001$), respectively, for thrombus detection. For MBIR images, these values were 14.3 (sensitivity, 0.916; specificity, 0.900; AUC, 0.976; $P < .0001$) for endoleak detection and 16.1 (sensitivity, 0.959; specificity, 0.925; AUC, 0.986; $P < .0001$) for thrombus detection.

Discussion

In our study, we systematically analyzed the effect of reduced-dose CT angiographic protocols with varying tube energies in conjunction with automated tube current modulation and different reconstruction algorithms on endoleak and in-stent thrombus conspicuity for the thoracic aorta. The advantages of using low tube energy in CT angiography have been thoroughly discussed in the literature; iterative algorithms in combination with reduced tube energy are able to offer a further decrease in CT-associated patient exposure to radiation.

Early detection and anatomic localization of small contrast media extravasations and recognition of an increase in the size of these extravasations are

Figure 4

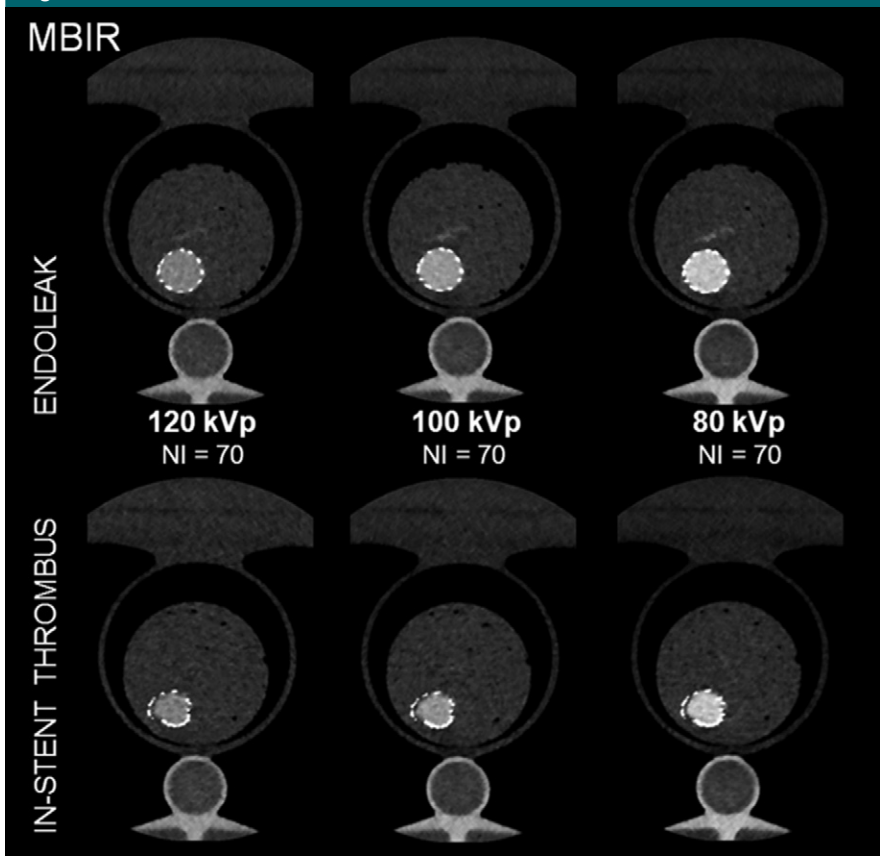

Figure 4: CT angiographic images show simulated endoleak and in-stent thrombus with the fully iterative algorithm. On MBIR images acquired with an NI of 70 at 100 and 80 kVp, the readers reliably identified small endoleaks; at 120 kVp, the readers deemed the presence of endoleaks questionable. With an NI of 70, thrombus detection was sufficient only at 80 kVp; the answers of two of five readers were unsure at 120 kVp, and two of five answers were false-positive at 100 kVp.

Figure 3

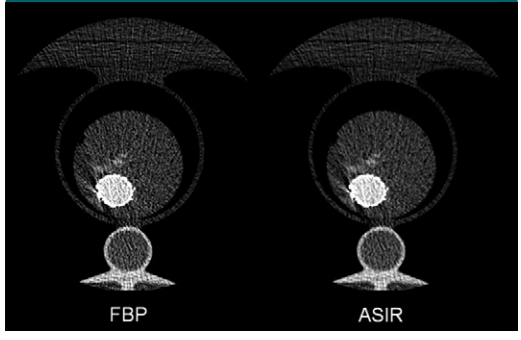

Figure 3: CT angiographic images show simulated endoleaks at 80 kvp. Medium endoleaks were identifiable with both FBP and ASIR by using an NI of 70 corresponding to a CT dose index value of 0.54 mGy.

Table 4

Attenuation and SNR in the Aorta

Tube Energy and NI	FBP		ASIR		MBIR		FBP		ASIR		MBIR	
	Attenuation (HU)	*P* Value	Attenuation (HU)	*P* Value	Attenuation (HU)	*P* Value	SNR	*P* Value	SNR	*P* Value	SNR	*P* Value
120 kVp												
16	247 ± 2.6	NA	247 ± 2.5	NA	246 ± 1.4	NA	9.5 ± 0.6	NA	12.0 ± 1.6	NA	21.2 ± 2.2	NA
25	246 ± 3.3	>.999	246 ± 3.2	>.999	245 ± 1.8	>.999	5.9 ± 0.3	NA	7.9 ± 0.8	.0043	19.2 ± 1.7	<.0001
34	248 ± 2.0	.99	249 ± 2.8	.91	247 ± 2.0	>.999	4.4 ± 0.3	NA	6.6 ± 0.5	.0035	16.1 ± 1.7	<.0001
43	247 ± 5.0	>.999	247 ± 4.7	>.999	245 ± 2.0	>.999	3.7 ± 0.2	NA	4.9 ± 0.3	<.0001	15.3 ± 1.5	<.0001
52	252 ± 5.4	.53	251 ± 6.2	.58	246 ± 2.3	>.999	2.8 ± 0.2	NA	3.7 ± 0.3	<.0001	13.7 ± 1.4	<.0001
61	245 ± 3.3	.99	252 ± 5.1	.32	242 ± 4.9	.27	2.4 ± 0.2	NA	3.3 ± 0.3	<.0001	12.8 ± 1.6	.0023
70	252 ± 6.7	.68	252 ± 6.4	.69	240 ± 5.9	.31	1.9 ± 0.1	NA	2.6 ± 0.2	<.0001	10.8 ± 0.8	.0072
100 kVp												
16	308 ± 1.8	NA	308 ± 1.8	NA	311 ± 2.0	NA	11.5 ± 0.9	NA	15.2 ± 1.5	NA	26.8 ± 3.4	NA
25	306 ± 2.5	.50	306 ± 2.6	.61	306 ± 2.2	.0011	6.9 ± 0.4	NA	9.3 ± 0.7	.0017	23.5 ± 3.3	<.0001
34	305 ± 2.4	.37	305 ± 2.3	.30	304 ± 2.0	<.0001	5.8 ± 0.3	NA	7.6 ± 0.7	<.0001	19.0 ± 0.9	<.0001
43	306 ± 4.5	.99	306 ± 4.7	.98	302 ± 3.1	<.0001	4.4 ± 0.3	NA	5.9 ± 0.5	<.0001	17.5 ± 2.0	<.0001
52	308 ± 7.1	>.999	308 ± 6.6	>.999	298 ± 2.1	<.0001	3.4 ± 0.5	NA	4.4 ± 0.7	<.0001	16.8 ± 2.4	<.0001
61	311 ± 6.8	.99	311 ± 6.5	.99	296 ± 2.3	<.0001	2.5 ± 0.2	NA	3.3 ± 0.3	<.0001	15.7 ± 1.4	<.0001
70	314 ± 8.2	.83	313 ± 8.0	.89	290 ± 2.8	<.0001	2.4 ± 0.2	NA	3.2 ± 0.2	<.0001	13.5 ± 1.1	.0010[2]
80 kVp												
16	400 ± 2.9	NA	400 ± 2.9	NA	400 ± 2.7	NA	15.1 ± 1.3	NA	20.2 ± 2.1	NA	33.6 ± 3.2	NA
25	398 ± 3.2	.99	398 ± 3.0	.98	394 ± 2.2	.0007	8.7 ± 0.6	NA	11.5 ± 0.8	<.0001	28.4 ± 2.2	<.0001
34	396 ± 2.4	.38	396 ± 2.4	.35	394 ± 2.9	.0002	7.1 ± 0.5	NA	9.6 ± 0.7	<.0001	22.8 ± 1.8	<.0001
43	397 ± 3.8	.99	397 ± 3.3	.93	391 ± 2.1	<.0001	5.8 ± 0.2	NA	7.8 ± 0.2	<.0001	21.9 ± 1.4	<.0001
52	405 ± 4.1	.17	405 ± 3.7	.14	388 ± 1.9	<.0001	4.2 ± 0.2	NA	5.5 ± 0.2	<.0001	21.7 ± 1.2	<.0001
61	401 ± 6.3	>.999	402 ± 5.9	>.999	381 ± 2.9	<.0001	3.2 ± 0.2	NA	4.3 ± 0.3	<.0001	20.1 ± 2.8	.0006
70	402 ± 5.7	.99	402 ± 5.6	.99	369 ± 2.5	<.0001	2.9 ± 0.3	NA	4.0 ± 0.4	<.0001	19.4 ± 2.1	.0007

Note.—Data are mean ± standard deviation. Attenuation of the aorta measured with low-dose protocols was compared with the corresponding value obtained with the control protocol with the same reconstruction algorithm and tube energy. NA = not applicable.

important when differentiating between endoleaks that are dangerous or progressive and those that are stable. Because of the well-known limitations of magnetic resonance angiography and US, CT angiography remains the preferred modality in the follow-up of patients after EVAR. It has been shown that type II endoleaks with a diameter larger than 15 mm are associated with aneurysm expansion (28). In our phantom, the smallest endoleak was 2×6 mm.

In our study, detectability of the simulated vascular disease was ensured with FBP at 120 kVp with an NI of 25 instead of 16 corresponding to a noise level higher than that suggested by the manufacturer. When the tube energy was lowered to 100 or 80 kVp, the tolerable noise level increased, and radiation dose was reduced by 43% and 58%, respectively. The hybrid algorithm allowed for moderately higher SNR values in the aorta and better detection of the simulated lesions than did FBP. Its noise reduction effect seemed to be weaker at 80 kVp than at 100 or 120 kVp. The fully iterative algorithm increased SNR and improved lesion conspicuity more powerfully than did the hybrid algorithm. In comparison to FBP, it decreased radiation dose by 66% at 120 kVp, 69% at 100 kVp, and 63% at 80 kVp. The extended reconstruction time still represents an important drawback of the fully iterative algorithm.

In our phantom study, we observed certain threshold values for SNR of the aorta relating to endoleak or in-stent thrombus conspicuity. In comparison with the hybrid algorithm or FBP, the threshold value for endoleak detection was higher for the images obtained with the fully iterative algorithm (14.3 for MBIR vs 5.5 for FBP and 6.6 for ASIR). Furthermore, this algorithm required a higher threshold to depict in-stent thrombus with high specificity than to identify endoleaks (16.1 for MBIR vs 5.1 for FBP and 4.7 for ASIR). These results indicate the limited reliability of image noise in the evaluation and comparison of the fully iterative algorithm with other algorithms concerning image quality analysis.

An important finding of our study is the significant decrease in CT attenuation measured in the aorta (up to 20 HU at 100 kVp, up to 31 HU at 80 kVp) that we detected on images obtained with the fully iterative algorithm and use of decreased dose and tube energies. This shift might be associated with the altered noise spectral density, which is a special feature of the algorithm that seems to affect CT attenuation if low tube energy is used and intensified quantum noise is present (16).

Our study had limitations. Because this was a phantom study, we noted only moderate variation in endoleak and thrombus morphology in comparison with the large variety of vascular diseases in patients. We used only one CT system; therefore, results might not be applicable to systems from different vendors. We used only one phantom size that was not representative of all patients. Finally, the evaluation was based on the subjective impression of the five radiologists and the reference standard of a full-dose diagnostic CT scan interpreted by one investigator.

In conclusion, the results of our experimental phantom suggest that use of low tube energy in combination with a fully iterative reconstruction algorithm enables definitive, more pronounced dose reduction with the three algorithms. This technique seems suitable for imaging surveillance of endoleak and in-stent thrombus at considerably reduced radiation exposure, without the impairment of lesion conspicuity in the thoracic aorta. Our phantom data offer preliminary parameters with which to introduce CT angiography protocols applying a relatively low radiation exposure with the aid of low-tube-voltage and NI-guided tube current modulation using either filtered back projection or partially or fully iterative algorithms in clinical routine.

Disclosures of Conflicts of Interest: Z.D. No relevant conflicts of interest to disclose. **J.G.** Financial activities related to the present article: none to disclose. Financial activities not related to the present article: gave scientific presentations for GE Healthcare. Other relationships: none to disclose. **F.M.** No relevant conflicts of interest to disclose. **L.L.G.** Financial activities related to the present article: none to disclose. Financial activities not related to the present article: gave lectures and served on speakers bureaus for GE Healthcare. Other relationships: none to disclose. **M.T.** Financial activities related to the present article: none to disclose. Financial activities not related to the present article: is a consultant for Covidien, Biotronik, and Endoscout. Other relationships: none to disclose. **M.F.R.** No relevant conflicts of interest to disclose. **S.W.** Financial activities related to the present article: none to disclose. Financial activities not related to the present article: institution received a general scientific grant from GE Healthcare, gave educational and scientific presentations for GE Healthcare. Other relationships: none to disclose.

References

1. Desai ND, Burtch K, Moser W, et al. Long-term comparison of thoracic endovascular aortic repair (TEVAR) to open surgery for the treatment of thoracic aortic aneurysms. J Thorac Cardiovasc Surg 2012;144(3):604–609; discussion 609–611.
2. Czerny M, Funovics M, Sodeck G, et al. Long-term results of thoracic endovascular aortic repair in atherosclerotic aneurysms involving the descending aorta. J Thorac Cardiovasc Surg 2010;140(6,Suppl):S179–S184; discussion S185–S190.
3. Mustafa ST, Sadat U, Majeed MU, Wong CM, Michaels J, Thomas SM. Endovascular repair of nonruptured thoracic aortic aneurysms: systematic review. Vascular 2010;18(1):28–33.
4. Morales JP, Greenberg RK, Lu Q, et al. Endoleaks following endovascular repair of thoracic aortic aneurysm: etiology and outcomes. J Endovasc Ther 2008;15(6):631–638.
5. Alsac JM, Khantalin I, Julia P, et al. The significance of endoleaks in thoracic endovascular aneurysm repair. Ann Vasc Surg 2011;25(3):345–351.
6. Stavropoulos SW, Charagundla SR. Imaging techniques for detection and management of endoleaks after endovascular aortic aneurysm repair. Radiology 2007;243(3):641–655.
7. Ricotta JJ 2nd. Endoleak management and postoperative surveillance following endovascular repair of thoracic aortic aneurysms. J Vasc Surg 2010;52(4 Suppl):91S–99S.
8. Zoli S, Trabattoni P, Dainese L, et al. Cumulative radiation exposure during thoracic endovascular aneurysm repair and subsequent follow-up. Eur J Cardiothorac Surg 2012;42(2):254–259; discussion 259–260.
9. Fleischmann D, Boas FE. Computed tomography: old ideas and new technology. Eur Radiol 2011;21(3):510–517.

10. May MS, Wüst W, Brand M, et al. Dose reduction in abdominal computed tomography: intraindividual comparison of image quality of full-dose standard and half-dose iterative reconstructions with dual-source computed tomography. Invest Radiol 2011;46(7):465–470.

11. Silva AC, Lawder HJ, Hara A, Kujak J, Pavlicek W. Innovations in CT dose reduction strategy: application of the adaptive statistical iterative reconstruction algorithm. AJR Am J Roentgenol 2010;194(1):191–199.

12. Gervaise A, Osemont B, Lecocq S, et al. CT image quality improvement using Adaptive Iterative Dose Reduction with wide-volume acquisition on 320-detector CT. Eur Radiol 2012;22(2):295–301.

13. Winklehner A, Karlo C, Puippe G, et al. Raw data-based iterative reconstruction in body CTA: evaluation of radiation dose saving potential. Eur Radiol 2011;21(12):2521–2526.

14. Katsura M, Matsuda I, Akahane M, et al. Model-based iterative reconstruction technique for radiation dose reduction in chest CT: comparison with the adaptive statistical iterative reconstruction technique. Eur Radiol 2012;22(8):1613–1623.

15. Vardhanabhuti V, Loader RJ, Mitchell GR, Riordan RD, Roobottom CA. Image quality assessment of standard- and low-dose chest CT using filtered back projection, adaptive statistical iterative reconstruction, and novel model-based iterative reconstruction algorithms. AJR Am J Roentgenol 2013;200(3):545–552.

16. Singh S, Kalra MK, Do S, et al. Comparison of hybrid and pure iterative reconstruction techniques with conventional filtered back projection: dose reduction potential in the abdomen. J Comput Assist Tomogr 2012;36(3):347–353.

17. Pickhardt PJ, Lubner MG, Kim DH, et al. Abdominal CT with model-based iterative reconstruction (MBIR): initial results of a prospective trial comparing ultralow-dose with standard-dose imaging. AJR Am J Roentgenol 2012;199(6):1266–1274.

18. Suzuki S, Machida H, Tanaka I, Ueno E. Measurement of vascular wall attenuation: comparison of CT angiography using model-based iterative reconstruction with standard filtered back-projection algorithm CT in vitro. Eur J Radiol 2012;81(11):3348–3353.

19. Scheffel H, Stolzmann P, Schlett CL, et al. Coronary artery plaques: cardiac CT with model-based and adaptive-statistical iterative reconstruction technique. Eur J Radiol 2012;81(3):e363–e369.

20. Nakayama Y, Awai K, Funama Y, et al. Lower tube voltage reduces contrast material and radiation doses on 16-MDCT aortography. AJR Am J Roentgenol 2006;187(5):W490–W497.

21. Funama Y, Taguchi K, Utsunomiya D, et al. Combination of a low-tube-voltage technique with hybrid iterative reconstruction (iDose) algorithm at coronary computed tomographic angiography. J Comput Assist Tomogr 2011;35(4):480–485.

22. McCollough CH, Bruesewitz MR, Kofler JM Jr. CT dose reduction and dose management tools: overview of available options. RadioGraphics 2006;26(2):503–512.

23. Kanal KM, Stewart BK, Kolokythas O, Shuman WP. Impact of operator-selected image noise index and reconstruction slice thickness on patient radiation dose in 64-MDCT. AJR Am J Roentgenol 2007;189(1):219–225.

24. Söderberg M, Gunnarsson M. Automatic exposure control in computed tomography: an evaluation of systems from different manufacturers. Acta Radiol 2010;51(6):625–634.

25. Boone JM, Strauss KJ, Cody D, et al. Size-specific dose estimates (SSDE) in pediatric and adult body CT examinations. AAPM Report No. 204. College Park, Md: American Association of Physicists in Medicine, 2011.

26. Szucs-Farkas Z, Semadeni M, Bensler S, et al. Endoleak detection with CT angiography in an abdominal aortic aneurysm phantom: effect of tube energy, simulated patient size, and physical properties of endoleaks. Radiology 2009;251(2):590–598.

27. Deák Z, Grimm JM, Treitl M, et al. Filtered back projection, adaptive statistical iterative reconstruction, and a model-based iterative reconstruction in abdominal CT: an experimental clinical study. Radiology 2013;266(1):197–206.

28. Timaran CH, Ohki T, Rhee SJ, et al. Predicting aneurysm enlargement in patients with persistent type II endoleaks. J Vasc Surg 2004;39(6):1157–1162.